Highly luminescent cesium lead halide perovskite nanocrystals with tunable composition and thickness by ultrasonication

Highly Luminescent Cesium Lead Halide Perovskite Nanocrystals with Tunable Composition and Thickness via Ultrasonication

Yu Tong,[a] Eva Bladt,[b] Meltem F. Aygüler,[c] Aurora Manzi,[a] Karolina Z. Milowska,[d] Verena A. Hintermayr,[a] Pablo Docampo,[c] Sara Bals,*[b] Alexander S. Urban,*[a] Lakshminarayana Polavarapu,*[a] Jochen Feldmann[a]

Abstract: We present a simple, scalable, single-step and polar-solvent-free synthesis of high quality colloidal $CsPbX_3$ (X=Cl, Br and I) perovskite nanocrystals (NCs) with tunable halide ion composition and thickness by direct ultrasonication of the corresponding precursor solutions in the presence of organic capping molecules. High angle annular dark field scanning transmission electron microscopy (HAADF-STEM) reveals the atomically resolved cubic crystal structure and surface termination of the NCs. The NCs exhibit high photoluminescence quantum yields (PLQY), narrow emission line widths, and considerable air stability. In addition, we investigate the quantum size effect in $CsPbBr_3$ and $CsPbI_3$ nanoplatelets by tuning their thickness down to only 3-6 monolayers. The high quality of the prepared NCs ($CsPbBr_3$) is demonstrated through amplified spontaneous emission with low thresholds. Furthermore, versatility of this synthesis approach is demonstrated by applying to different kinds of perovskite NCs.

The outstanding optoelectronic properties of inexpensive and solution processable metal hybrid halide perovskites have brought them into the forefront of many research fields such as solar cells, light emitting diodes, photodetectors and lasers.[1] One of the main advantages of this material is the large and easy tunability of the optical bandgap through exchange of the individual components.[2] The success of this material led to the expansion into nanocrystals (NCs), first in the form of organic/inorganic hybrid perovskites,[1b, 3] and later also into purely inorganic cesium based NCs.[4] Nanocrystals exhibit high PLQY and they offer an inherent way to tune the optical properties due to size- and dimensionality- dependent quantum confinement.[5] Currently, only a limited number of synthetic methods are available for the preparation of $CsPbX_3$ NCs as compared to conventional metal chalcogenide-based NCs. The most widely used method for the preparation of $CsPbX_3$ nanocubes with very high PLQY is based on high temperature hot injection, which was developed by Kovalenko and co-workers in 2015 and refined by Alivisatos and co-workers to obtain nanoplatelets (NPLs).[6] However, the hot injection approach is tedious, it is generally performed under an inert atmosphere and can currently only be applied to thickness control of Br-based perovskites. Indeed, a halide ion exchange step is necessary to prepare nanoplatelets comprising iodide or chloride perovskites, as shown simultaneously by Manna and co-workers. [6-7] In addition, Sun et al.[8] reported shape control synthesis of $CsPbBr_3$ NCs at room temperature. However, this method require the pre-synthesis of Cs-precursor under inert atmosphere at higher temperatures. Despite being simple, room temperature synthesis suffers with the production of NCs that exhibit relatively low PLQY NCs.[8] Herein, we report a versatile, polar-solvent-free and single step approach for the large scale synthesis of highly luminescent $CsPbX_3$ perovskite NCs and NPLs. We demonstrate that both the halide composition and the NPLs thickness is tunable by direct ultrasonication of the corresponding precursors in the presence of organic ligands (Figure1a). The ability to tune the thickness revealed the quantum size effects in $CsPbX_3$ (X=Br and I) NPLs. This has enabled us to investigate the thickness dependent optical properties of $CsPbI_3$ NPLs for the first time.

As shown in Figure 1a, our synthesis of $CsPbX_3$ (X=Cl, Br and I) perovskite NCs is based on direct tip sonication of corresponding precursor salts (Cs_2CO_3 and PbX_2) together with capping ligands (oleylamine and oleic acid) in a nonpolar solvent (mineral oil or octadecene) under ambient atmospheric conditions. Previously such a sonication process has been used for the preparation of metal nanoparticles. This method takes the advantage of metal-ligand complex formation under ultrasonication, which then further reduce into metal nanoparticles. In the present system, sonication induces the formation of a Cs-oleate complex that is soluble in nonpolar solvents and reacts with PbX_2 in the presence of oleylamine and oleic acid to obtain colloidal $CsPbX_3$ NCs in a single pot directly from their precursors (Figure S1). Figure 1b shows the purified colloidal dispersions of $CsPbX_3$ (X=Cl, Br, I, Cl/Br and Br/I) perovskite NCs in hexane under room light as well as UV light. The PL emission colour varies from blue to green to red as the composition of the precursors is varied from Cl to Br to I (Figure 1b & S1). The synthesis is easily scaled up by multiplying each of the reaction components. The optical properties of the

[a] Y. Tong, A. Manzi, Dr. A. Urban, Dr. L. Polavarapu, and Prof. Dr. J.Feldmann
Photonics and Optoelectronics Group
Department of Physics and Center for NanoScience (CeNS), Ludwig-Maximilians-Universität
Amalienstr.54, 80799, Munich, Germany
E-mail: urban@lmu.de & l.polavarapu@lmu.de

[b] B. Eva, Prof.Dr. S. Bals
EMAT
University of Antwerp
Groenenborgerlaan 171, B-2020 Antwerp, Belgium
E-mail: sara.bals@uantwerpen.be

[c] M. Ayguler and Prof. Dr. Pablo Docampo
Department of Chemistry and Center for NanoScience (CeNS), Ludwig-Maximilians-Universität (LMU), Butenandtstraße 5- 13, 81377 Munich, Germany.

[d] Dr. Karolina Z. Milowska
Department of Materials Science and Metallurgy, University of Cambridge, 27 Charles Babbage Rd, Cambridge CB3 0FS, UK.

Supporting information for this article is given via a link at the end of the document.

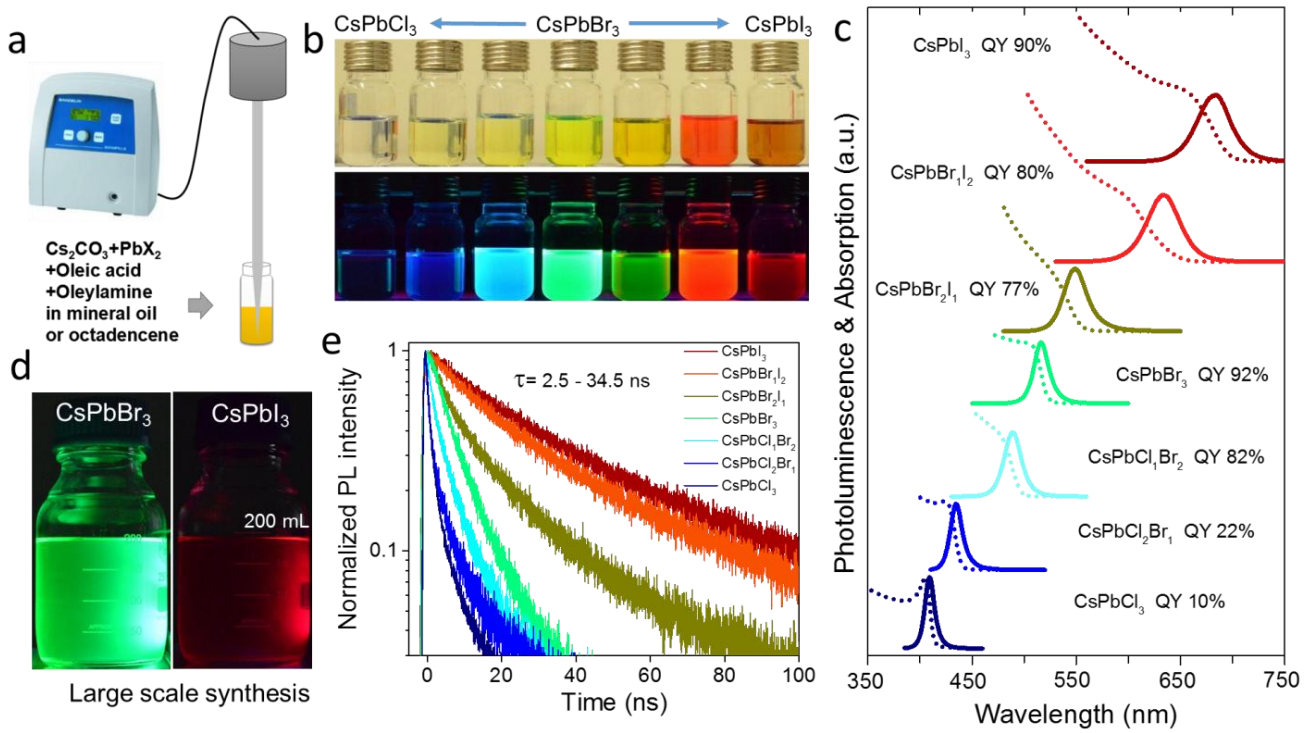

Figure 1. (a) Schematic illustration of the synthesis of $CsPbX_3$ NCs through single-step tip-sonication. (b) Photograph of colloidal dispersions of $CsPbX_3$ NCs with different halide (x=Cl, Br and I) compositions in hexane under room light (top) and UV light (bottom, λ= 367 nm). (c) Corresponding UV-vis and PL spectra, and PLQYs of samples shown in (b). (d) Scalable synthesis of NCs (scaled up to 10 times). Photograph of $CsPbBr_3$ and $CsPbI_3$ colloidal dispersions under UV light. (e) PL decay dynamics of NCs shown in (b) (calculated τ~2.5-34.5 ns).

colloidal dispersions obtained in this manner hardly differ from those of the original synthesis (Figure 1c and S2).

UV-vis absorption and fluorescence spectroscopy was performed to quantify the observations of the color change upon varying the halide content (Figure 1c). The prepared dispersions exhibit narrow, single peak PL emission (FWHM~12-40 nm). The UV-vis spectra show a single, steep absorption onset, only slightly red shifted from the PL maximum. These observations clearly show that the dispersions only contain a single material and not NCs with varying halide content and that the optical band gap energy can be tuned nearly across the entire visible range (~410-700 nm) by adjusting the halide composition. Moreover, the samples with pure Br or I exhibit high PL quantum yields (QYs) over 90%, while the mixed halides $CsPbBr_xCl_{3-x}$, with x≥ 2 had considerably lower PLQY of only 10-25% (Figure 1c). Additionally, it was found that all colloidal dispersions except $CsPbI_3$ appear to be stable for several methods with a slight reduction in their PLQYs (Figure S3 and Table S1). Whereas $CsPbI_3$ NCs gradually transformed into non-fluorescent yellow phase after 2 months of storage under atmospheric conditions. Previously it has been shown that mixed halide organic/inorganic perovskite NCs exhibit phase separation under light illumination,[9] however these inorganic perovskite seems to be stable under continuous light excitation (Figure S4). Time-resolved PL measurements of $CsPbX_3$ NCs present multiexponential decay traces with average lifetimes in the range of 2.5-34.4 ns and with an inverse correlation between halide ions controlled bandgap and decay lifetime. Combining the PL decay time together with the PLQY values shows that while the iodide- and bromide-containing NCs are of high optical quality with nearly vanishing non-radiative decay, the NCs with high chloride content show significant non-radiative decay. The observed trend in the PLQYs and decay rates can be ascribed to intrinsic optical properties of halide perovskites.[2c]

Further proof of the high quality of the prepared nanocrystals can be seen by electron microscopy. Bright field transmission electron microscopy (BF-TEM) overview images of $CsPbBr_3$ (Figure 2a) and $CsPbI_3$ (Figure 2d) NCs show well-defined cubic and rectangular shapes in projection (see Figure S5 for TEM images of mixed halide perovskite NCs). The average size range of the crystals are ~10-15 nm and ~8-12 nm for $CsPbBr_3$ and $CsPbI_3$, respectively. The prepared $CsPbBr_3$ NCs are rather monodisperse with an average size of 14.3±1.3 nm, which is slightly higher than the NCs (~11 nm) obtained through hot injection method (Figure S6).[4f] By terminating the synthesis at specific reaction times and by acquiring TEM images of the $CsPbBr_3$ NCs present in each solution, we find that the particle size gradually increases with reaction time, indicating a seeded growth (Figure S7). The crystal structure of the different NCs was investigated by HAADF-STEM imaging. In Figure 2b, an atomic resolution HAADF-STEM image of a $CsPbBr_3$ NCs acquired along the [100] direction shows that the NC is single crystalline and exhibits a cubic crystal structure with a lattice parameter of 5.9 Å (Figure 2c). The presence of Cs, Pb and Br in $CsPbBr_3$ NC was confirmed by energy dispersive X-ray spectroscopy (EDX) mapping (Figure S8). Like their bromide counterparts, the $CsPbI_3$ NCs were found to exhibit high crystallinity and a cubic crystal structure with a lattice spacing of 6.3 Å (Figure 2e,f). It is well known that $CsPbX_3$ NCs can crystallize in cubic, tetragonal and orthorhombic polymorphs of the perovskite crystal lattice. By analyzing the crystal structure of a significant number of particles using high resolution HAADF-STEM, we found that all the NCs are single crystals and exhibit mostly the cubic perovskite phase regardless of morphology (Figure S9) or composition (Figure S10), further confirmed by

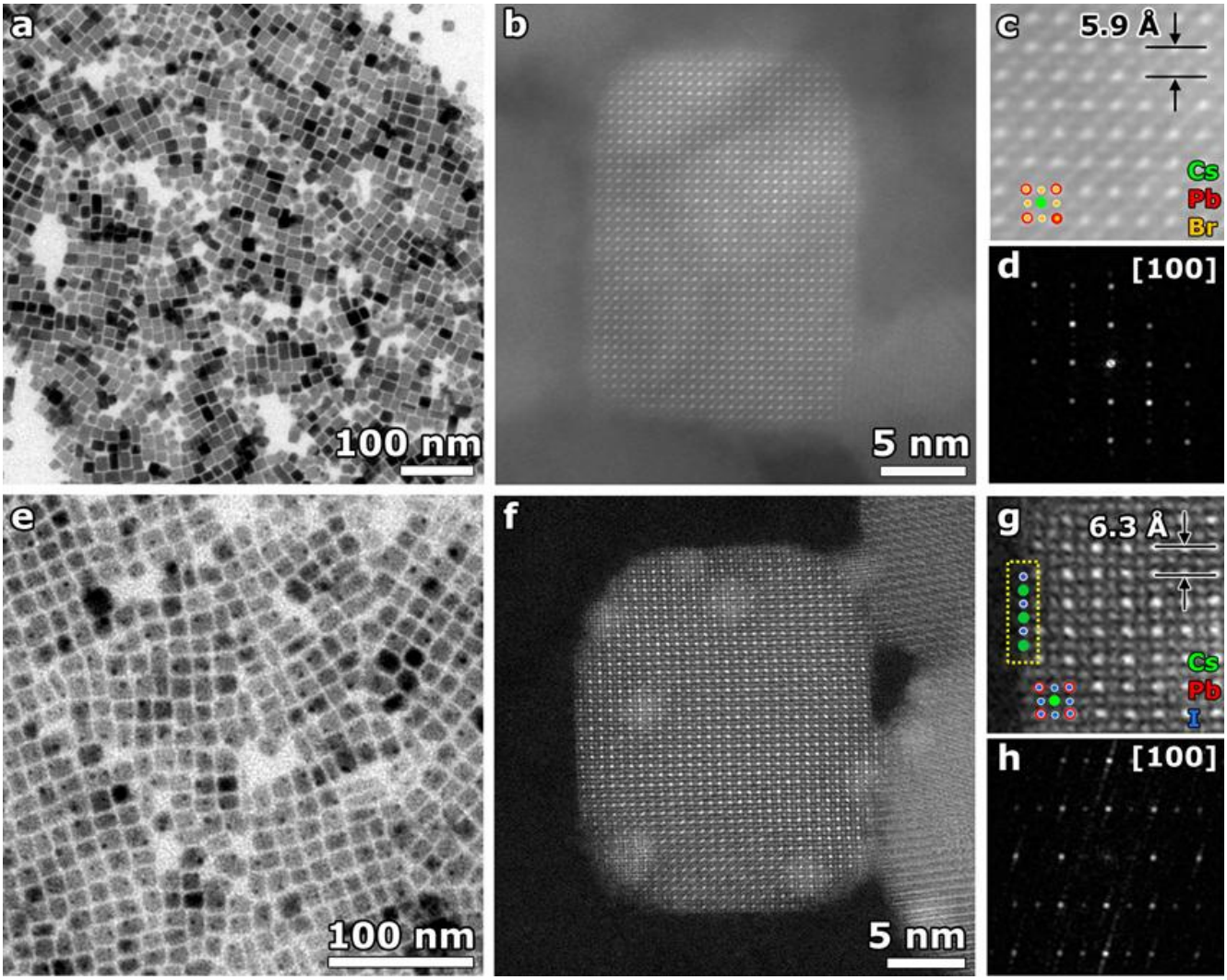

Figure 2 (a,d) BF-TEM overview images of $CsPbBr_3$ and $CsPbI_3$ NCs, respectively. (b,e) Atomically resolved high resolution HAADF-STEM image of a single $CsPbBr_3$ and a CsPbI3 NC with (c,f) a more detailed view, respectively.

XRD measurements performed on nanocrystalline thin films (Figure S11) and powders (Figure S12). Interestingly, from the detailed view of the HAADF-STEM image of the iodide NC in Figure 2f, we can suggest that the surface termination consists of Cs and I ions (Figure 2f & Figure S13). This provides some hints about the ligand binding mechanism, which so far has not been fully understood. Since the crystal terminates with Cs atoms, it is most likely that the NCs are passivated by Cs-bound alkyl chains, e.g. Cs-oleate (Figure S13).

Interestingly, while varying the initial conditions of the synthesis, we found that we were able to change the fluorescence of the dispersions from a dark red to a bright orange for the case of $CsPbI_3$ NCs. By reducing the ratio of Cs_2CO_3 to PbI_2 we are able to blue-shift the resulting emission of the perovskite dispersions, with some of the dispersions displaying extremely broad PL spectra with multiple high energy emission peaks (Figure 3a). The newly emerging peaks do not shift position as the precursor ratio is changed, but rather their relative intensities change. In the extreme case, we are left with a single PL peak at 600 nm, constituting a nearly 100 nm shift from the original PL maximum at 685 nm. Additionally, in UV-Vis measurements we see a pronounced excitonic peak emerging, slightly redshifted from the respective PL maxima. To investigate the origin of this PL, we have recorded the TEM images the NCs of each sample (Figures 3b-e, cf. Figure S14). For the initial sample (1:3 precursor ratio), we see the cubic-looking NCs with sizes of 10-12 nm. As the Cs_2CO_3 content is reduced, we begin to see very thin structures together with cubic-shaped NCs. The lower the Cs content becomes, the larger the amount of these nanostructures is and the thickness becomes both thinner and less polydisperse. In the extreme case we find a nearly homogeneous distribution of nanocrystals of 10 x 2 nm size. These remind strongly of perovskite nanoplatelets (NPLs). Additionally, as the precursor ratio is varied, additional scattering peaks emerge at low angles in XRD measurements (Figure S14 and tables 2-4), a strong indicator of 2D nanocrystal formation.[10] It has been demonstrated previously by two groups that $CsPbBr_3$ NPLs with controlled thickness could be prepared by performing the NC growth at low temperatures.[4b, 11] In our method, it is most likely that the lower cesium content reduces the reaction rate and strongly favor 2D growth producing NPLs. To our knowledge, our work here constitutes the first report on the direct synthesis of highly fluorescent (~75% PLQY) $CsPbI_3$ NPLs with controlled thickness, enabling an understanding of the thickness-dependent excitonic properties of $CsPbI_3$ NPLs for the first time.

To validate the claim of NPLs as the source of the blue-shifted PL, we plot the position of the individual PL maxima versus the projected thickness of the NPLs responsible and apply a theoretical model to compare to the experimental data. The lowest experimentally observed PL peak is ascribed to a

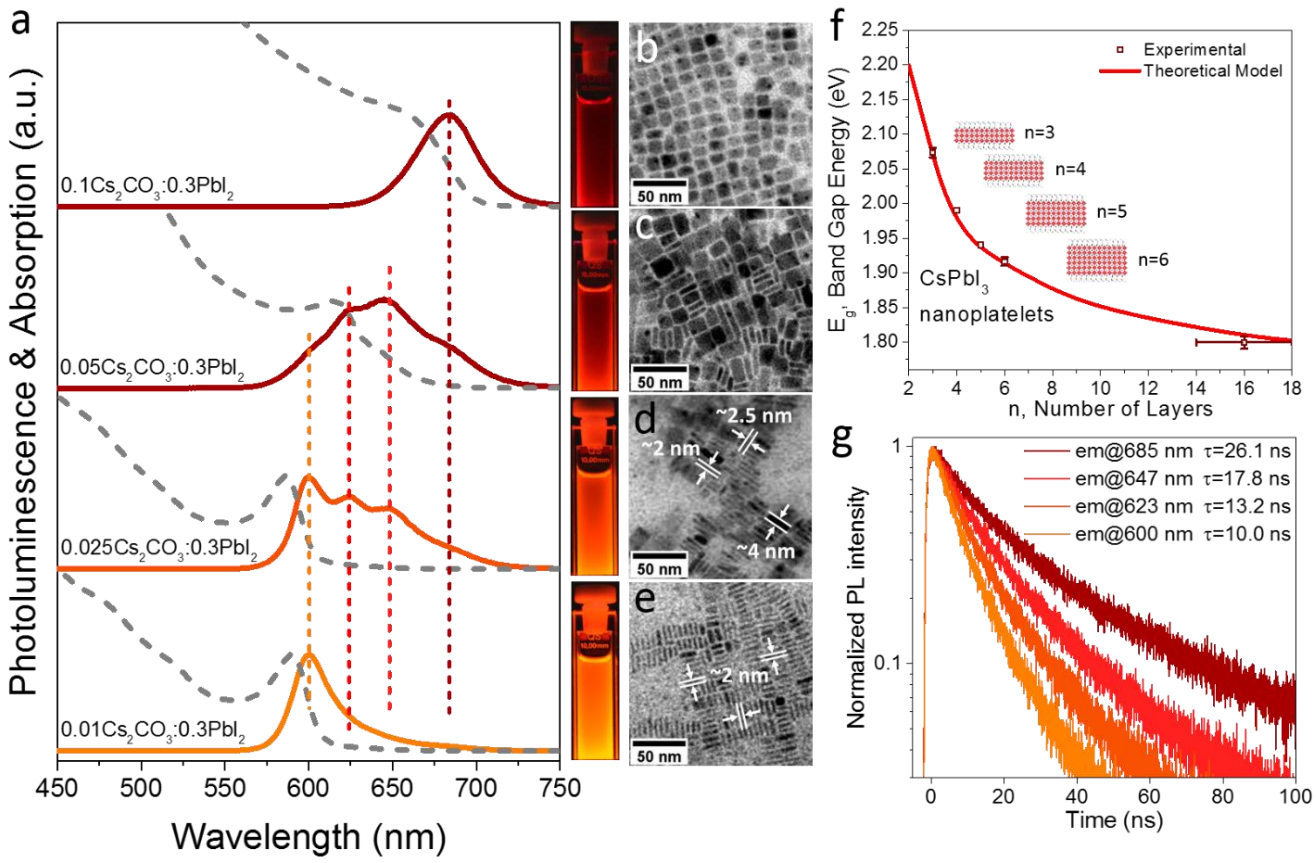

Figure 3. Tuning the optical properties by thickness control: UV-vis absorption and PL spectra of $CsPbI_3$ NCs prepared with different ratios of Cs_2CO_3 to PbI_2 precursors (a) and corresponding TEM images (b-e). (f) Calculated and experimental bandgap energies of perovskite nanoplatelets as a function of number of unit cells of perovskite nanoplatelets. (g) PL dynamics of a mixture of $CsPbI_3$ nanoplatelets of different thicknesses (prepared with Cs_2CO_3:PbI_2 = 0.025:0.3 mmol) probed at their peak positions (λ_{max}=600, 623, 647 and 685 nm)

three layers thick NPL, so with n = 3, as the ~2 nm from the TEM images are in excellent agreement with the expected thickness of 3 unit cells (~1.89 nm). Higher order peaks were then ascribed to incrementally thicker NPLs (Figure 3a, Figure S15). HAADF-STEM imaging of an intermediate sample displaying multiple emission peaks confirmed the presence of cubic phase single crystalline nanoplatelets (Figure S16, S17). The thickness of the platelets, which was found to vary from 4 to 6 unit cells, was determined from high resolution HAADF-STEM images of standing platelets (Figure, S17). We note that the platelets are extremely sensitive to the electron beam and they tend to degrade and loose their crystallinity during acquisition (Figure S18). By high-resolution HAADF-STEM imaging we are able to identify the emerging spherical nanoparticles as lead particles (Figure S19), as seen previously for the organic inorganic perovskites.[5a] For the bulk-like NCs we estimated the mean thickness to be 16 layer, corresponding to the roughly 10 nm large NCs. An established theoretical model was used to calculate the expected PL positions (See Supporting Information for details).[5a] We find an extremely good agreement between the experimental results and our calculations (Figure 3f), showing that the NCs observed in the dispersions are in fact producing the observed fluorescence. Time-resolved PL measurements were performed on the NPL colloidal dispersions, which were diluted enough to prevent both non-radiative energy transfer and reabsorption of PL in the dispersion. Shown for the case of a sample with many PL peaks (0.025 mmol Cs_2CO_3), we probe the PL decay at the PL peaks corresponding to the NPLs of individual thicknesses using TCSPC coupled with monochrometor. We find that the traces show a multiexponential form with average lifetimes between 27 and 10 ns and decreasing with decreasing thickness of the nanoplatelets likely due to increase in exciton binding energy in the strongly confined nanostructures (Figure 3g). This behavior is similar to that seen in epitaxial GaAs quantum wells.[12] Additionally, we show that this synthesis process is applicable to the preparation of $CsPbBr_3$ nanoplatelets (Figure S20). We obtain similar results with blue-shifted PL peaks emerging in the highly emissive dispersions. We are again able to correlate this emission to theoretical values, showing the thickness dependence.

The high PL QY and large absorption cross-sections of the NCs suggests they should be promising for lasing applications with low thresholds for optical gain.[5h] To this end, we have investigated the emergence of amplified spontaneous emission (ASE) in films comprising $CsPbBr_3$ NCs (Figure 4). Exciting the NCs at 400 nm with a femtosecond-pulsed laser, we see the normal PL signal at low fluences. At higher laser powers a new, narrow peak (full width half maximum, FWHM;3-7 nm) emerges on the low-energy shoulder of the PL peak, redshifted by about 15-20 nm due to band gap renormalization, and rapidly increasing in intensity as the pump power is increased (Figure 4a). By plotting the integrated intensity of the fluorescence versus the pump fluence, we see a clear threshold behavior with an onset for ASE at 2.1 μJ/cm² (Figure 4b). This is comparable to values reported for $CsPbX_3$ NCs prepared by using hot-injection technique [5h] and lower than the values reported for surface-passivated $CsPbBr_3$ NCs.[13] Our studies clearly demonstrate that these NCs are excellent candidates light-emitting applications. In an attempt to remove the lead, one of the remaining large challenges in the perovskite field,[14] we have applied this synthesis for the preparation of $CsSnBr_3$ nanocrystals, which were highly monodisperse, but proved to be

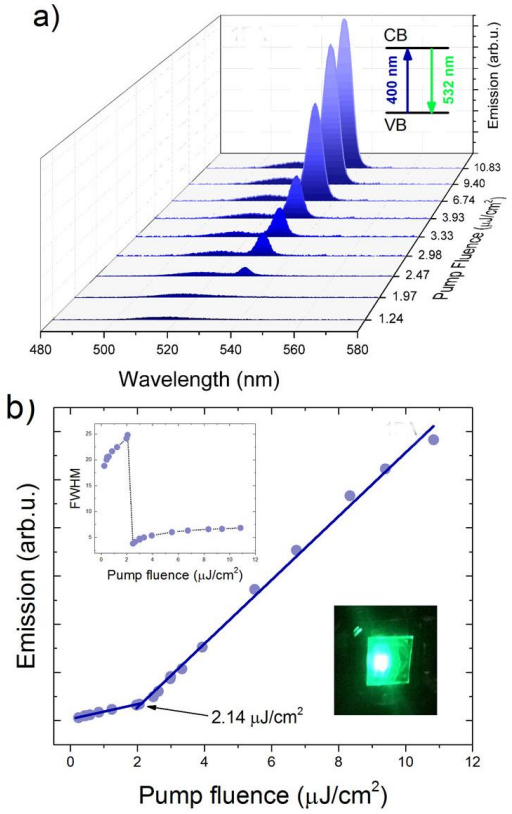

Figure 4. Pump-fluence dependent PL emission (evolution of ASE) from $CsPbBr_3$ NC film (a) and corresponding emission intensity at 530 nm (b), and FWHM (inset of b). All the spectra are obtained with 400 nm femtosecond laser excitation.

slightly unstable (Figure S21). Additionally, the versatility of this synthesis approach is further demonstrated by applying to the preparation of $CH_3NH_3PbBr_3$ NCs (Figure S22).

In summary, we have presented a polar solvent-free and scalable single-step solution phase synthesis of highly luminescent $CsPbX_3$ perovskite NCs with photoluminescence tunable across the visible spectrum (~400-700 nm). The cubic crystallinity and atomically precise surface termination of NCs are revealed by high resolution HAADF-STEM imaging. In addition, we have shown the quantum size effect in $CsPbBr_3$ and $CsPbI_3$ nanoplatelets. That fact that these NCs exhibit low threshold ASE is further proof of their high quality. Importantly, we have demonstrated that this simple synthesis approach can be extended, with all of the components replaceable.

Acknowledgements

This work was supported by the Bavarian State Ministry of Science, Research, and Arts through the grant "Solar Technologies go Hybrid (SolTech)", by the China Scholarship Council (Y.T.), by the Alexander von Humboldt-Stiftung (L.P.), by European Union through the award of a Marie Curie Intra-European Fellowship (P.D.), by the Scientific and Technological Research Council of Turkey (M.A.), by Flemish Fund for Scientific Research (FWO Vlaanderen) (E.B.). S.B. acknowledges financial support from European Research Council (ERC Starting Grant #335078-COLOURATOMS).

Keywords: Perovskite nanocrystals and nanoplatelets • $CsPbX_3$ • ultrasonication • quantum confinement • HAADF-STEM

[1] a) M. M. Lee, J. Teuscher, T. Miyasaka, T. N. Murakami, H. J. Snaith, *Science* **2012**, *338*, 643-647; b) L. C. Schmidt, A. Pertegas, S. Gonzalez-Carrero, O. Malinkiewicz, S. Agouram, G. M. Espallargas, H. J. Bolink, R. E. Galian, J. Perez-Prieto, *J. Am. Chem. Soc.* **2014**, *136*, 850-853.

[2] a) V. D'Innocenzo, A. R. Srimath Kandada, M. De Bastiani, M. Gandini, A. Petrozza, *J. Am. Chem. Soc.* **2014**, *136*, 17730-17733; b) G. E. Eperon, S. D. Stranks, C. Menelaou, M. B. Johnston, L. M. Herz, H. J. Snaith, *Energy Environ. Sci.* **2014**, *7*, 982-988; c) Q. A. Akkerman, V. D'Innocenzo, S. Accornero, A. Scarpellini, A. Petrozza, M. Prato, L. Manna, *J. Am. Chem. Soc.* **2015**, *137*, 10276-10281.

[3] a) S. Gonzalez-Carrero, R. E. Galian, J. Perez-Prieto, *J Mater Chem A* **2015**, *3*, 9187-9193; b) H. Huang, A. S. Susha, S. V. Kershaw, T. F. Hung, A. L. Rogach, *Adv. Sci.* **2015**, *2*, 1500194; c) F. Zhang, H. Zhong, C. Chen, X.-g. Wu, X. Hu, H. Huang, J. Han, B. Zou, Y. Dong, *ACS Nano* **2015**, *9*, 4533-4542; d) B. Luo, Y.-C. Pu, S. A. Lindley, Y. Yang, L. Lu, Y. Li, X. Li, J. Z. Zhang, *Angew. Chem. Int. Ed.* **2016**, *55*, 8864-8868.

[4] a) A. Swarnkar, R. Chulliyil, V. K. Ravi, M. Irfanullah, A. Chowdhury, A. Nag, *Angew. Chem. Int. Ed.* **2015**, *54*, 15424-15428; b) Y. Bekenstein, B. A. Koscher, S. W. Eaton, P. D. Yang, A. P. Alivisatos, *J. Am. Chem. Soc.* **2015**, *137*, 16008-16011; c) X. Li, Y. Wu, S. Zhang, B. Cai, Y. Gu, J. Song, H. Zeng, *Adv. Funct. Mater.* **2016,** *26*, 2435–2445; d) J. Song, J. Li, X. Li, L. Xu, Y. Dong, H. Zeng, *Adv. Mater.* **2015**, *27*, 7162-7167; e) Y. Wang, X. Li, J. Song, L. Xiao, H. Zeng, H. Sun, *Adv. Mater.* **2015**, *27*, 7101-7108; f) L. Protesescu, S. Yakunin, M. I. Bodnarchuk, F. Krieg, R. Caputo, C. H. Hendon, R. X. Yang, A. Walsh, M. V. Kovalenko, *Nano Lett.* **2015**, *15*, 3692-3696.

[5] a) J. A. Sichert, Y. Tong, N. Mutz, M. Vollmer, S. Fischer, K. Z. Milowska, R. García Cortadella, B. Nickel, C. Cardenas-Daw, J. K. Stolarczyk, A. S. Urban, J. Feldmann, *Nano Lett.* **2015**, *15*, 6521-6527; b) P. Tyagi, S. M. Arveson, W. A. Tisdale, *J. Phys. Chem. Lett.* **2015**, *6*, 1911-1916; c) D. Di, K. P. Musselman, G. Li, A. Sadhanala, Y. Ievskaya, Q. Song, Z.-K. Tan, M. L. Lai, J. L. MacManus-Driscoll, N. C. Greenham, R. H. Friend, *J. Phys. Chem. Lett.* **2015**, *6*, 446-450; d) F. Zhu, L. Men, Y. Guo, Q. Zhu, U. Bhattacharjee, P. M. Goodwin, J. W. Petrich, E. A. Smith, J. Vela, *ACS Nano* **2015**, *9*, 2948-2959; e) F. Palazon, F. Di Stasio, Q. A. Akkerman, R. Krahne, M. Prato, L. Manna, *Chem. Mater.* **2016**, *28*, 2902-2906; f) S. Pathak, N. Sakai, F. Wisnivesky Rocca Rivarola, S. D. Stranks, J. Liu, G. E. Eperon, C. Ducati, K. Wojciechowski, J. T. Griffiths, A. A. Haghighirad, A. Pellaroque, R. H. Friend, H. J. Snaith, *Chem. Mater.* **2015**, *27*, 8066-8075; g) J. Song, J. Li, X. Li, L. Xu, Y. Dong, H. Zeng, *Adv. Mater.* **2015**, *27*, 7162-7167; h) S. Yakunin, L. Protesescu, F. Krieg, M. I. Bodnarchuk, G. Nedelcu, M. Humer, G. De Luca, M. Fiebig, W. Heiss, M. V. Kovalenko, *Nat. Commun.* **2015**, *6*, 8056.

[6] a) L. Protesescu, S. Yakunin, M. I. Bodnarchuk, F. Krieg, R. Caputo, C. H. Hendon, R. X. Yang, A. Walsh, M. V. Kovalenko, *Nano Lett.* **2015**, *15*, 3692-3696; b) Y. Bekenstein, B. A. Koscher, S. W. Eaton, P. Yang, A. P. Alivisatos, *J. Am. Chem. Soc.* **2015**, *137*, 16008-16011.

[7] Q. A. Akkerman, S. G. Motti, A. R. Srimath Kandada, E. Mosconi, V. D'Innocenzo, G. Bertoni, S. Marras, B. A. Kamino, L. Miranda, F. De Angelis, A. Petrozza, M. Prato, L. Manna, *J. Am. Chem. Soc.* **2016**.

[8] S. Sun, D. Yuan, Y. Xu, A. Wang, Z. Deng, *ACS Nano* **2016**, *10*, 3648-3657.

[9] E. T. Hoke, D. J. Slotcavage, E. R. Dohner, A. R. Bowring, H. I. Karunadasa, M. D. McGehee, *Chem. Sci.* **2015**, *6*, 613-617.

[10] a) S. Gonzalez-Carrero, G. M. Espallargas, R. E. Galian, J. Perez-Prieto, *J. Mater. Chem. A* **2015**, *3*, 14039-14045; b) Z. Yuan, Y. Shu, Y. Tian, Y. Xin, B. Ma, *Chem. Commun.* **2015**, *51*, 16385-16388.

[11] Q. A. Akkerman, S. G. Motti, A. R. Srimath Kandada, E. Mosconi, V. D'Innocenzo, G. Bertoni, S. Marras, B. A. Kamino, L. Miranda, F. De Angelis, A. Petrozza, M. Prato, L. Manna, *J. Am. Chem. Soc.* **2016**, *138*, 1010-1016.

[12] J. Feldmann, G. Peter, E. O. Gobel, P. Dawson, K. Moore, C. Foxon, R. J. Elliott, *Phys. Rev. Lett.* **1987**, *59*, 2337-2340.

[13] J. Pan, S. P. Sarmah, B. Murali, I. Dursun, W. Peng, M. R. Parida, J. Liu, L. Sinatra, N. Alyami, C. Zhao, E. Alarousu, T. K. Ng, B. S. Ooi, O. M. Bakr, O. F. Mohammed, *J. Phys. Chem. Lett.* **2015**, *6*, 5027-5033.

[14] M. A. Green, A. Ho-Baillie, H. J. Snaith, *Nat. Photonics* **2014**, *8*, 506-514.